Obrabotka metallov (tekhnologiya, oborudovanie, instrumenty) = Metal Working and Material Science. 2026 vol. 28 no. 1 pp. 152–175
ISSN: 1994-6309 (print) / 2541-819X (online)
DOI: 10.17212/1994-6309-2026-28.1-152-175

NSTU NETI

Obrabotka metallov -
Metal Working and Material Science

Journal homepage: http://journals.nstu.ru/obrabotka_metallov

Turning Inconel 718 with a self-propelled rotary tool using a hybrid nanofluid under minimum quantity lubrication

Satish Chinchanikar [1, a, *], ***Nitin Motgi*** [2, 3, b]

[1] Department of Mechanical Engineering, Vishwakarma Institute of Technology, Affiliated to Savitribai Phule Pune University, Pune – 411037, India
[2] Department of Mechanical Engineering, Vishwakarma Institute of Information Technology, Affiliated to Savitribai Phule Pune University, Pune – 411048, India
[3] Department of Mechanical Engineering, D.Y. Patil International University, Akurdi, Pune, Maharashtra, 411044, India

[a] https://orcid.org/0000-0002-4175-3098, satish.chinchanikar@vit.edu; [b] https://orcid.org/0000-0001-9062-8341, nitin.221p0031@viit.ac.in

ARTICLE INFO

Article history:
Received: 05 November 2025
Revised: 22 November 2025
Accepted: 17 December 2025
Available online: 15 March 2026

Keywords:
Turning
Inconel 718
MQL
Rotary tool
Nanofluid

ABSTRACT

Introduction. Superalloys like nickel ones are crucial in aircraft construction, rocket production, and, more broadly, in the aviation industry due to their hard-wearing, and high-strength properties, but high machining temperatures pose challenges to their machinability. Manufacturers are always looking for new ways to improve these materials' machinability using cutting-edge cutting tool technologies and suitable cooling methods. In this context, rotary tools have shown significant potential for better performance in machining challenging materials. ***The purpose of the work.*** It is essential to comprehend geometric dimensioning and tolerance (*GD&T*) parameters when machining aerospace alloys to ensure precision and interchangeability in parts manufacturing. However, limited studies have investigated these parameters while considering the effect of nanofluids during turning with rotary tools. **Methods of investigation.** This study explores the turning of *Inconel 718* with a hybrid nanofluid under minimum quantity lubrication (*NFMQL*) conditions using a self-propelled rotary tool (*SPRT*). Nanofluids were prepared by mixing Al_2O_3 and multi-walled carbon nanotubes in palm oil. The analysis of worn tools was performed through optical and *SEM* images. Further, the radial *GD&T* parameters, such as circularity, cylindricity, radial runout, surface roughness, tool life, and workpiece hardness, are discussed as they vary with the cutting conditions. Additionally, the technique for order of preference by similarity to the ideal solution (*TOPSIS*) in association with a genetic algorithm (*GA*) was used to generate *Pareto* solutions and select the optimal compromise solution. The work with the optimized parameters is finally summarized. **Results and Discussion.** A hybrid nanofluid under *NFMQL* conditions was used to assess the processability of *Inconel 718* during turning with an *SPRT*. The circularity, cylindricity, radial runout, and machined surface characteristics were investigated. The worn tools have been examined through optical and scanning electron microscopy images. Surface roughness and tool life are significantly affected by feed and cutting speed, while cylindricity is strongly impacted by the depth of cut. *Pareto* fronts and the best compromise solutions were obtained using a genetic algorithm integrated with *TOPSIS*. This study found that turning *Inconel 718* at a feed rate and depth of cut of 0.1 mm/rev and 0.2 mm, respectively, and a cutting speed between 30–60 m/min could achieve circularity and cylindricity deviations of up to 5.68 μm and radial runout of up to 0.43 mm, as well as surface roughness, tool life, and workpiece hardness in the ranges of 1.07–1.54 μm, 3.46–8.44 min, and 36–38 HRC, respectively. This research provides valuable insights for designing an *SPRT* and promoting its wide adoption and application in the machining domain for machining superalloys. This study suggests exploring nanoparticle agglomeration in nanofluids and the use of additives to improve machining efficiency. Additionally, this research identifies opportunities to enhance machining performance under *NFMQL* conditions by utilizing micro-textured *SPRTs* with nanofluids, addressing concerns related to machined surface integrity.

For citation: Chinchanikar S., Motgi N. Turning Inconel 718 with a self-propelled rotary tool using a hybrid nanofluid under minimum quantity lubrication. *Obrabotka metallov (tekhnologiya, oborudovanie, instrumenty) = Metal Working and Material Science*, 2026, vol. 28, no. 1, pp. 152–175. DOI: 10.17212/1994-6309-2026-28.1-152-175. (In Russian).

*** Corresponding author**
Satish Chinchanikar, Ph.D. (Engineering), Professor
Department of Mechanical Engineering,
Vishwakarma Institute of Information Technology,
Affiliated to Savitribai Phule Pune University, Pune – 411048, India
Tel.: 91-2026950401, **e-mail:** satish.chinchanikar@vit.edu

Introduction

Superalloys, such as those based on titanium and nickel, are crucial in aircraft and rocket manufacturing, as well as in the aviation industry in general, due to their wear resistance, strength, and durability. However, the high temperatures generated during their machining pose significant challenges to their machinability [1, 2]. Manufacturers are constantly looking for new methods to improve the machinability of these materials by employing advanced cutting tool technologies and effective cooling strategies [3].

In response to government regulations and health concerns, researchers are using minimum quantity lubrication (*MQL*) to reduce heat generation and mitigate its adverse effects on machinability. To overcome the relatively low heat transfer efficiency of base fluids, various attempts have been made to enhance their thermal performance by dispersing nanoparticles within them. The high thermal conductivity of nanoparticles significantly improves the heat transfer capability of the base fluids [4]. The study of nanofluids is rapidly gaining prominence due to their unique chemical, mechanical, and thermal properties, which contribute to environmental and industrial sustainability. Nevertheless, a critical factor influencing machinability is the type of base fluid and the concentration of nanoparticles within it [5].

A number of studies have assessed the machinability of nickel alloys using unitary and hybrid nanofluids (a mix of different nanoparticles, such as graphene, carbon nanotubes, and copper oxides, with base fluids including methanol, water, machine oils, vegetable oils, and synthetic oils) [6]. Nanofluids based on multi-walled carbon nanotubes (*MWCNTs*) and aluminum oxide (Al_2O_3) provided better performance during the turning of nickel alloys owing to their higher cooling capacity and lower wettability [7, 8]. *Makhesana* and *Patel* [9] used a nanofluid of molybdenum disulfide (MoS_2) nanoparticles dispersed in palm oil to machine *Inconel 718* under *MQL*. Their investigation found that, compared to other machining conditions, a 1 % concentration of MoS_2 nanoparticles in palm oil reduced tool wear and surface roughness.

Rotary tools have shown significant potential for improving tool life and surface quality when machining difficult-to-cut materials. Researchers have found that the insert in a self-propelled rotary tool (*SPRT*), which rotates around its axis, distributes wear and heat evenly along the cutting edge, thus increasing tool life [10]. Due to the enhanced cooling and continuous engagement of the workpiece with a fresh segment of the cutting edge, the *SPRT* demonstrated superior machining performance in numerous comparative studies with conventional stationary tools [11, 12]. Furthermore, research shows that rotary cutting significantly enhances tool life due to uniform wear distribution, reduced effective cutting speed, and improved heat transfer [13].

Researchers have optimized machining performance by determining the optimal *SPRT* geometry and dimensions, including insert diameters, inclination angles, rake angles, and clearance angles. They found that selecting the ideal insert angle, tool rotation speed, and tool diameter is pivotal for aligning the cutting force direction with the tool's stiffness [14–16]. Additionally, when designing an *SPRT*, the rigidity of the bearing unit integrated into the rotary tool holder must be considered to improve surface waviness and dimensional accuracy of the machined part [15–17].

Researchers are increasingly utilizing advanced optimization techniques to improve the machinability of *Inconel 718*, as traditional methods often struggle with contradictory objectives that must be considered collectively. Methods such as multi-criteria decision-making (*MCDM*) and evolutionary algorithms are widely used for multi-objective optimization. In one such hybrid approach, the technique for order preference by similarity to ideal solution (*TOPSIS*) is integrated with the genetic algorithm (*GA*) for this purpose [8, 18–21].

A hybrid *GA-TOPSIS* approach was used in previous studies [8, 18] to optimize turning parameters for *Inconel 718*. The findings demonstrated that the *GA* generated a wide range of feasible solutions, and *TOPSIS* successfully ranked them according to their desirability. These studies emphasized the significance of weight assignment in the *TOPSIS* approach and its sensitivity to the quality of the output. Using the *Taguchi*-grey relational analysis (*GRA*) and *TOPSIS* methodologies, *Rao* et al. [19] developed a multi-response optimization model for turning *Inconel 718*. Their comparative study demonstrates the effectiveness of the *Taguchi-GRA* approach for optimizing the turning of nickel alloys. Other researchers have optimized the turning of *Inconel 718* using various techniques such as *TOPSIS*, *DEAR* (Data Envelopment Analysis Ranking), and *GRA*. All these methods proved effective in identifying similar optimal parameters [20, 21].

Very little research has been conducted on the machining of *Inconel 718* using *SPRT*, despite its potential advantages. This limited research activity may be attributed to the restricted availability of rotary tools. It has been reported that the most common failure mode for *SPRTs* is chipping of the insert edge, resulting from mechanical and thermal shock induced by the continuous engagement of a fresh cutting edge throughout the machining process [13]. The existing literature indicates that the performance improvement achieved when machining *Inconel 718* with a rotary tool is not as substantial as that with titanium alloys. This is attributed to *Inconel 718*'s rapid work-hardening tendency, which shortens tool life. Additionally, studies showed that an *SPRT* must be sufficiently rigid to avoid insert run-out and machined surface waviness [12, 15–17].

A thorough understanding of geometric dimensioning and tolerancing (*GD&T*) parameters — such as circularity, cylindricity, and radial runout — is essential when machining aerospace alloys to ensure precision and part interchangeability in manufacturing. Tool chatter, a common mode of tool failure when machining difficult-to-cut alloys, significantly affects *GD&T* parameters. However, few studies have investigated *GD&T* parameters in the turning of *Inconel 718* [11, 12]. Further research into *GD&T* parameters during the machining of *Inconel 718*, considering the effects of process parameters, is required to ensure accurate manufacturing and proper assembly of parts.

The literature review reveals that the use of *SPRT*, while offering machinability benefits, can induce work hardening to a greater depth in the subsurface layer of the workpiece. Therefore, the ***goal of this work*** is to achieve improved tool life in rotary tool machining without compromising surface integrity. Additionally, only a limited number of studies have been reported on the turning of *Inconel 718* using nanofluids.

Therefore, this study investigates the turning of *Inconel 718* alloy with a hybrid nanofluid under *MQL* conditions using a self-propelled rotary carbide tool. Nanofluids were prepared by dispersing Al_2O_3 and *MWCNT* nanoparticles in palm oil at fixed concentrations. Tool wear analysis was performed using optical and *SEM* microscopy. Furthermore, the effects of cutting conditions on radial *GD&T* parameters (circularity, cylindricity, radial runout), surface roughness, tool life, and subsurface work hardening are analyzed. Moreover, *TOPSIS* coupled with *GA* was used to generate *Pareto*-optimal solutions and select the best compromise option. Finally, the results obtained with the optimized parameters are summarized.

Methods of investigation

Over the last decade, extensive research has been conducted on machining with nanofluids, prepared by dispersing various nanoparticles in a base fluid. The addition of nanoparticles to a base fluid enhances heat transfer efficiency, leading to improved machining performance. However, this requires careful consideration of nanoparticle agglomeration, which increases with concentration. This study involves the preparation of a hybrid nanofluid by dispersing Al_2O_3 and *MWCNT* nanoparticles in vegetable-based palm oil, selected for its superior thermal conductivity, lubricity, and anti-corrosive properties. The properties of the selected nanoparticles are provided in Table 1 [7].

Previous studies have shown that nanofluids based on Al_2O_3 and *MWCNT*s offer improved lubricity, contributing to enhanced machinability [22–24]. In the present study, the hybrid nanofluid was prepared via a two-step method, following the procedure outlined in [7] and illustrated in Fig. 1.

Mechanical stirring, probe ultrasonication, and magnetic stirring were employed to produce a surfactant-free hybrid nanofluid with homogeneously dispersed nanoparticles and no sedimentation. Ultrasonication breaks down nanoparticle agglomerates, while magnetic stirring maintains a homogeneous dispersion over time. The concentration of nanoparticles in the base fluid was determined based on pilot studies and a literature review to optimize the nanofluid's properties. While a higher nanoparticle concentration enhances heat transfer performance, it also increases fluid viscosity. *MWCNTs* exhibit greater density and viscosity

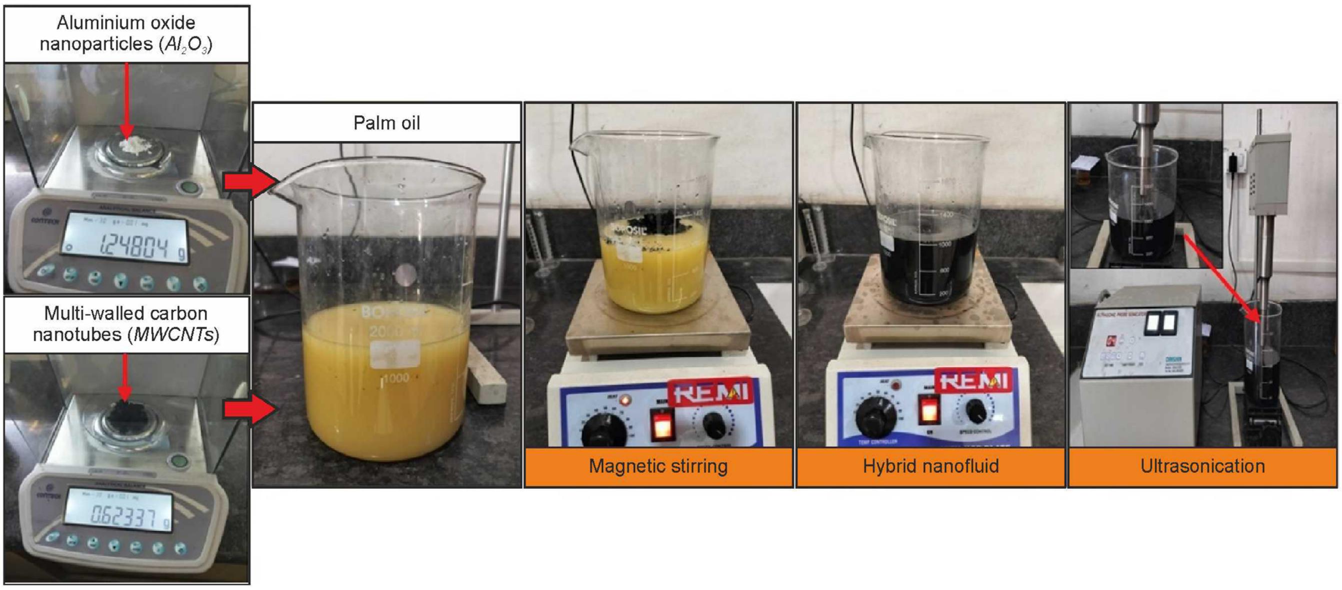

Fig. 1. Preparation of a hybrid nanofluid

than Al_2O_3 nanoparticles, whereas Al_2O_3 nanoparticles have a lower contact angle and higher thermal conductivity. To leverage their synergistic effects, *MWCNTs* and Al_2O_3 nanoparticles were mixed in equal volume proportions. In this study, a hybrid nanofluid with a total nanoparticle concentration of 0.25% by volume was prepared using vegetable-based palm oil as the base fluid.

The prepared nanofluid was first stirred at 700 rpm for 20 minutes to improve homogeneity. Subsequently, ultrasonication was performed using a probe sonicator for 30 minutes. Finally, a magnetic stirrer was used for 30 minutes to prevent nanoparticle sedimentation and ensure smooth fluid flow during the turning process. Table 1 presents the density, acid value, wettability, viscosity, surface tension, and thermal conductivity of the prepared hybrid nanofluid.

Table 1

Properties of nanoparticles and the hybrid nanofluid

Properties	Nanoparticles		Hybrid Al_2O_3+*MWCNTs* nanofluid	
	Al_2O_3	*MWCNTs*		
Purity	99.9%	99 %	Density (g/ml)	0.945
Average particle size (nm)	20–50	10–30	Viscosity (cP)	212
Average inner diameter (nm)	–	5–10	Acid value (KOH/g)	4.61
Average length/lateral dimension	–	5 nm	Surface tension (N/m)	43.02
Bulk density (g/cm^3)	0.5	0.04	Contact angle (^{o})	32.55
Morphology	Spherical	Tabular	Thermal conductivity (W/m^{o}C)	0.213
Color	White	Black		

Experimental Design

The tool life, surface roughness, and radial *GD&T* parameters were investigated during turning of *Inconel 718* using an *SPRT* and a hybrid Al_2O_3+*MWCNTs* nanofluid under minimum quantity lubrication (*MQL*) on a *CNC* lathe. The process parameters, as well as the rotary tool geometry and dimensions, were selected based on a preliminary study for the chosen workpiece-tool combination. The chemical composition of the workpiece material is provided in Table 2. Nine experimental trials were conducted with varying feed rates (0.1, 0.2, and 0.3 mm/rev), cutting speeds (30, 50, and 65 m/min), and depths of cut (0.2, 0.5, and 0.8 mm).

The trials were carried out with a rotary carbide tool. Fig. 2 shows the custom-designed *SPRT* used in this study. The *SPRT* incorporates a combined needle and thrust bearing system to support the rotating insert

Table 2

Chemical composition of *Inconel 718* (wt%)

C	*Cr*	*Al*	*Ti*	*P+S*	*Si+B*	*Ni*	*Mo*	*Mn*	*Nb+Ta*	*Co*	*Fe*
0.005	18.37	0.35	1.10	0.015	0.057	52.82	2.87	0.062	5.01	0.22	Balance

shaft, ensuring its alignment and stability under load, as well as tool precision during high-force machining operations. A *RCMT1606M0MP* rotary carbide round insert (diameter: 16 mm, thickness: 6 mm, clearance angle: 7°) was used. The tool holder's inclination and rake angles were set to 6° and 35°, respectively. Fig. 3 shows the experimental setup. Detailed operating instructions and specifications for the custom-designed *SPRT* are provided in reference [13].

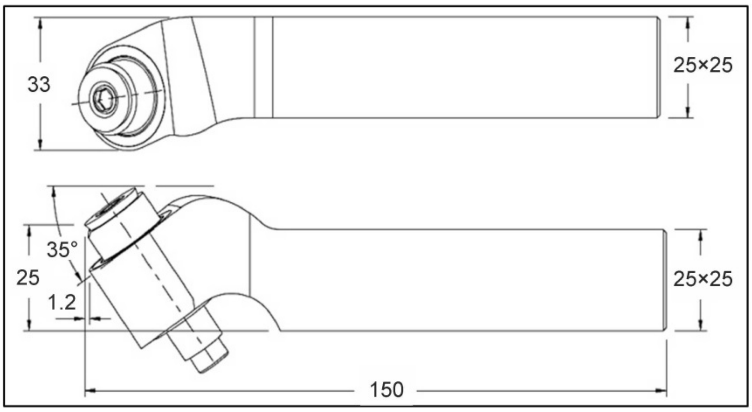

Fig. 2. Geometry of the self-propelled rotary tool

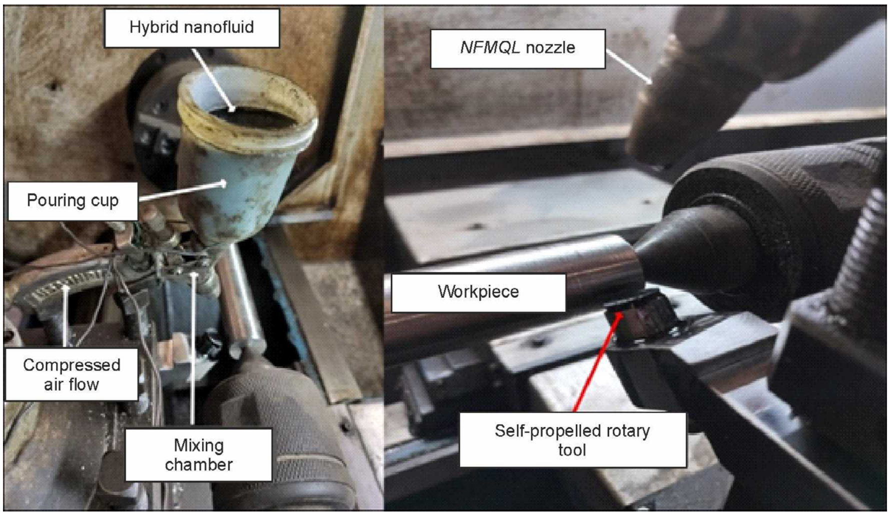

Fig. 3. Experimental setup

This study investigated the radial *GD&T* parameters – circularity, cylindricity, and radial runout – as a function of the cutting parameters. Circularity and cylindricity quantify the deviation of a feature from a perfect circle and cylinder, respectively. Circularity deviation is defined as the minimum radial separation between two concentric circles that enclose the actual profile of a cross-section. It is determined by analyzing a circular cross-section of a cylindrical part.

For critical components, circularity tolerances alone are insufficient to guarantee performance; cylindricity tolerances must also be specified to limit form deviations and ensure cylindrical form. Radial runout, on the other hand, is a two-dimensional tolerance that can be measured in either the axial or radial direction. It quantifies the deviation of a surface as the part rotates about a datum axis. Surface roughness was measured using a profilometer (*Mahr*, Model: *MarSurf M400*). The average roughness (***Ra***) value reported is the mean of measurements taken at four locations, spaced 90° apart, along the circumference of the specimen.

The hardness of the machined surface (work-hardened layer) was measured using a digital *Rockwell* hardness tester. Tool wear was assessed using a *Dino-Lite* digital microscope. Tool life was considered to have ended according to *ISO 3685* when flank wear reached 0.2 mm or in the event of catastrophic failure [1, 13]. Radial runout, cylindricity, and circularity (roundness) were measured using a bridge-type coordinate measuring machine (*CMM*) (*Carl Zeiss*, Model: *Contura*, Measuring range: 1,200×800×800 mm). Each experiment was repeated three times, and the presented results are the average values. To ensure measurement integrity, all tests were conducted at a controlled ambient temperature, and the equipment and specimens were cleaned with isopropyl alcohol and dried with lint-free towels prior to measurement.

Results and Discussion

This section presents the results analyzed through multi-objective optimization and mathematical modeling. The turning performance was evaluated based on radial *GD&T* parameters (circularity, cylindricity, and radial runout), tool life, surface roughness, and subsurface hardness. The influence of cutting parameters on tool wear mechanisms and chip morphology is also discussed. The average values of the investigated response variables are presented in Table 3.

Each experimental run was repeated three times, and the reported results represent the average of these measurements. Averaging was employed to ensure accuracy, account for process variability, and mitigate the influence of outliers. Data analysis revealed a 15–20% variation in the measured responses, indicating a degree of variability in the machining performance.

Circularity was measured on a single cross-section of the workpiece by rotating it about its axis to capture a complete profile. The circularity deviation, defined as the difference between the maximum and minimum radial distances, was determined from three profile measurements to identify errors and calculate the mean deviation. Cylindricity was evaluated by assessing the radial deviation between maximum and minimum values across multiple cross-sections along the cylinder's length. The cylindricity deviation was measured using the *CMM*'s software, which minimizes operator error by automating the recording of *X*, *Y*, and *Z* coordinates.

Tool wear was examined using an optical microscope, and the hardness of the machined subsurface layer was measured using a *Rockwell* hardness tester. The tester's digital system calculates hardness based on indentation depth, displaying the value directly to simplify readings and reduce human error. Figs. 4 and 5 show the variation in circularity and radial runout, respectively, across the different process conditions

Table 3

Test conditions and measured responses

Expt. run	*V* (m/min): *f* (mm/rev): *d* (mm)	Deviation in		Radial runout (*R*/*O*) (mm)	Surface roughness (*Ra*) (µm)	Tool life (*TL*) (min)	Work hardness (*HRC*)
		Circularity (*CIR*) (µm)	Cylindricity (*CYL*) (µm)				
R1	30:0.1:0.8	8.1	60.9	0.77	1.51	5.37	36.81
R2	30:0.3:0.8	9.2	72.8	1.07	2.44	3.91	37.67
R3	65:0.1:0.8	8	29.7	0.57	1.32	2.03	38.17
R4	65:0.3:0.8	9	66.7	0.64	1.63	1.12	39.56
R5	50:0.2:0.5	6.6	29.1	0.44	1.67	1.72	37.57
R6	30:0.1:0.2	3.3	10.1	0.19	1.48	8.42	36.25
R7	30:0.3:0.2	6.3	17.4	0.34	1.81	5.82	36.53
R8	65:0.1:0.2	2.9	7.5	0.11	1.05	3.81	38.65
R9	65:0.3:0.2	4.4	12.1	0.25	1.36	2.96	38.84

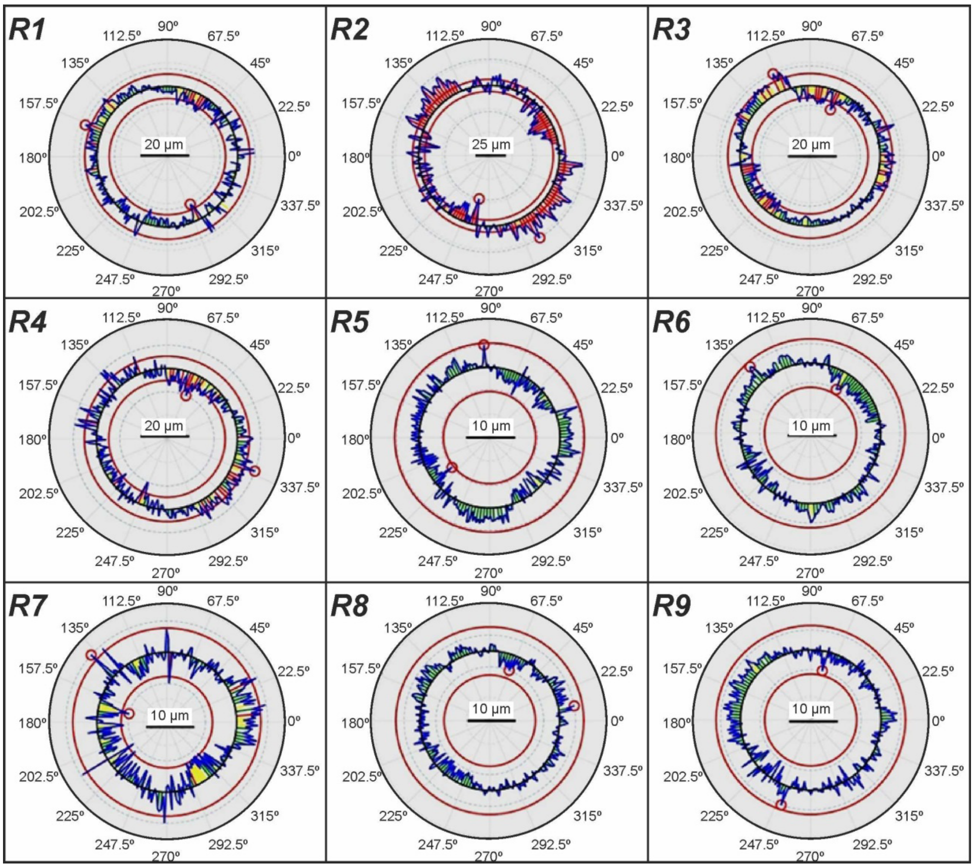

Fig. 4. Circularity deviation plots for different experimental runs (*R*1 to *R*9)

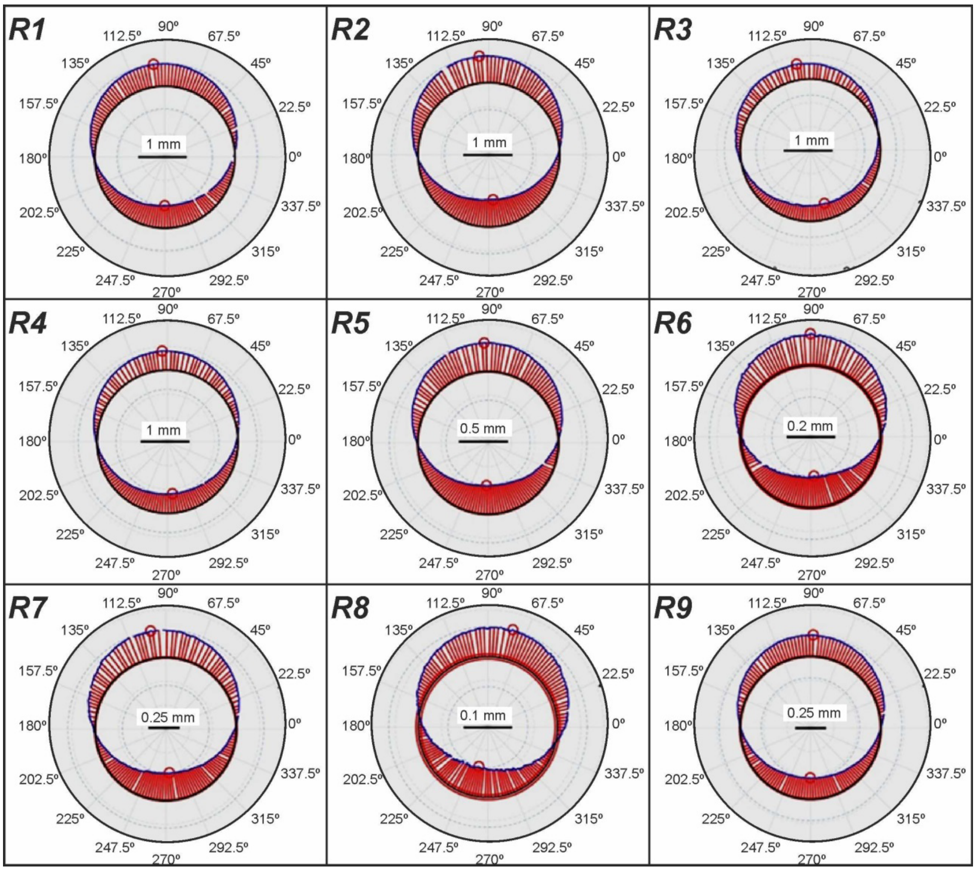

Fig. 5. Radial runout plots for different experimental runs (*R*1 to *R*9)

listed in Table 3. Mathematical models summarized in Table 4 were developed from the experimental data to analyze the influence of parameters on the studied responses. The unknown coefficients in the equations were determined using the *DataFit* software. Equations (1) to (6) in Table 4 represent the empirical models for predicting the investigated responses. The ***R***-squared values, all approximately 0.95, indicate that the models explain a significant portion of the variance in the dependent variables and can reliably predict responses during the turning of *Inconel 718*.

Table 4

Mathematical models for examined responses based on experimental data

Responses	Developed model	***R***-squared value	Eq. no.
Deviation in circularity (CIR) (μm)	$= 18.8735V^{-0.0963}f^{0.187}d^{0.4944}$	0.9144	(1)
Deviation in cylindricity (CYL) (μm)	$= 547.932V^{-0.3668}f^{0.361}d^{1.1768}$	0.9452	(2)
Radial runout (R/O) (mm)	$= 12.165V^{-0.566}f^{0.2681}d^{0.8842}$	0.9812	(3)
Surface roughness (Ra) (μm)	$= 12.73V^{-0.389}f^{0.2881}d^{0.1467}$	0.9211	(4)
Tool life (TL) (min)	$= 110.042V^{-1.152}f^{-0.3377}d^{-0.3648}$	0.96515	(5)
Work hardness (HRC)	$= 30.3477V^{0.0666}f^{0.0156}d^{0.0082}$	0.8825	(6)

To analyze the influence of input parameters on machining performance, graphical representations were generated using the empirical equations. The plots were created using a one-factor-at-a-time approach, varying one process parameter while keeping the others at their central (mid-level) values. This method allows for a systematic investigation of the individual effect of each parameter on the response variables. Isolating one parameter at a time simplifies the interpretation of its specific influence and facilitates data-driven decisions based on observed trends. Plots of the predicted responses, calculated using Eqs. (1)–(6), are presented in Figs. 6 and 7. For comparison, responses under dry cutting conditions, predicted by mathematical models developed for *SPRT* turning of *Inconel 718* [11], are also plotted in these figures.

Fig. 6 shows the variation of circularity (*CIR*) and cylindricity (*CYL*) deviations, as well as hardness, under both dry and *MQL* with nanofluid (*NFMQL*) conditions. The plots illustrate the effect of:

• Cutting speed (***V***) at a feed rate (***f***) of 0.2 mm/rev and depth of cut (***d***) of 0.5 mm.

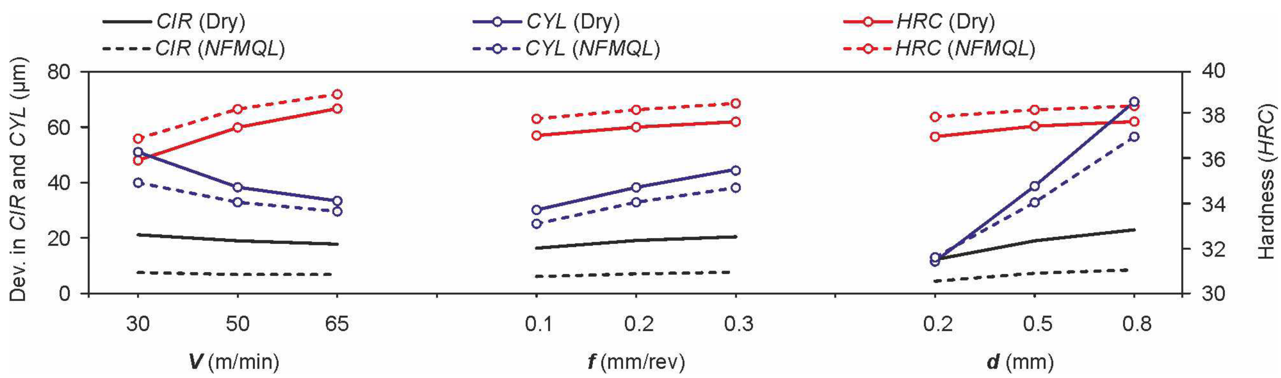

Fig. 6. Variation in deviation in circularity (*CIR*), cylindricity (*CYL*), and hardness (*HRC*) for dry and *NFMQL* conditions

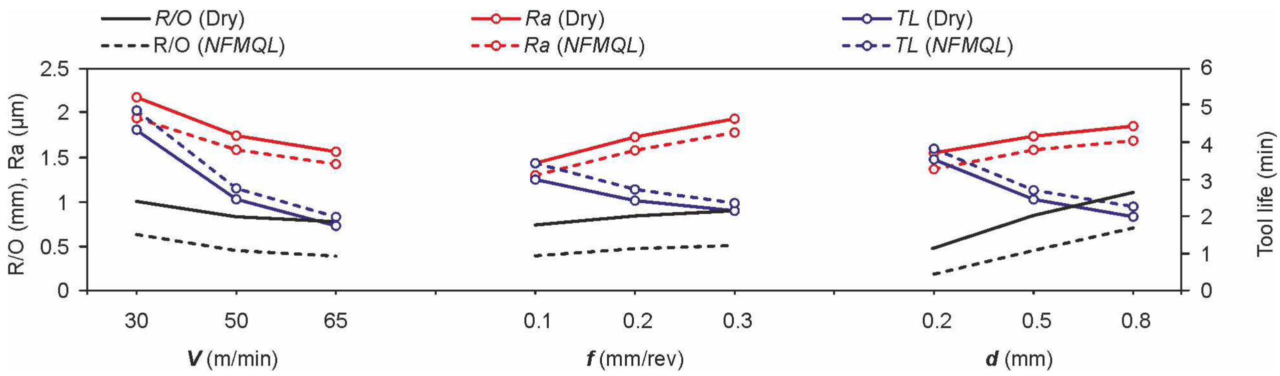

Fig. 7. Variation in radial runout (R/O), surface roughness (*Ra*), and tool life (*TL*) for dry and *NFMQL* conditions

• Feed rate (***f***) at a cutting speed (***V***) of 50 m/min and depth of cut (***d***) of 0.5 mm.
• Depth of cut (***d***) at a cutting speed (***V***) of 50 m/min and feed (***f***) of 0.2 mm/rev.

Fig. 7 shows the corresponding variation of radial runout (***R/O***), average surface roughness (***Ra***), and tool life (*TL*) under the same sets of conditions.

Analysis of Figs. 6 and 7 reveals that all investigated responses decrease with an increase in cutting speed (***V***), except for workpiece hardness. Tool life is significantly reduced by an increase in ***V***; therefore, prolonged tool life can be achieved by using lower cutting speeds. This effect is less pronounced under *NFMQL* conditions compared to dry turning. Conversely, superior results – namely, lower deviations in cylindricity and circularity, reduced surface roughness, and lower radial runout – are achieved at higher cutting speeds when using the hybrid nanofluid compared to dry conditions. Thus, increasing the cutting speed apparent as contradicting the investigating responses, especially the tool life with other *GD&T* parameters and surface roughness. Workpiece hardness appears to be only marginally influenced by cutting speed.

Higher cutting speeds generally result in lower surface roughness and smaller geometric deviations (cylindricity, radial runout, circularity). This can be attributed to the consequent increase in cutting zone temperature, which reduces material adhesion to the tool and prevents built-up edge formation, thereby minimizing surface irregularities. This leads to smoother and more precise surfaces. Additionally, the elevated temperature may locally soften the workpiece material near the cutting edge, facilitating smoother material removal, reducing cutting forces, and further improving surface finish and dimensional accuracy. Higher speeds also promote better chip flow and evacuation, preventing chip-induced surface damage and helping to maintain tight tolerances.

However, the elevated temperatures at higher cutting speeds can lead to tool softening, reducing the tool's hardness and strength. This increases the tool's susceptibility to wear and deformation, while also exacerbating wear mechanisms. The combination of high temperature and cutting forces predisposes the tool to chipping, fracture, and consequently, reduced tool life. These detrimental effects are more prominent in dry turning compared to turning under *NFMQL* conditions.

Figs. 6 and 7 show that tool life decreases, while the radial *GD&T* parameters and ***Ra*** increase with a rise in feed (***f***). An increase in feed thus presents a conflict between tool life and the other quality responses (*GD&T*, surface roughness). Conversely, all investigated responses increase with a rise in depth of cut (***d***), except for tool life. The *GD&T* parameters, particularly cylindricity followed by radial runout, are profoundly influenced by an increase in ***d***. Therefore, lower values for these parameters can be achieved by limiting the depth of cut. This effect is more pronounced during dry turning than under *NFMQL* conditions. Furthermore, superior performance – characterized by longer tool life and lower surface roughness and radial *GD&T* deviations – can be achieved under *NFMQL* conditions at reduced values of feed and depth of cut. The hardness of the machined workpiece is only marginally affected by these parameters.

The radial *GD&T* parameters are more sensitive to changes in depth of cut (***d***) than to feed rate (***f***) or cutting speed (***V***), especially during dry turning. This occurs because the depth of cut has a dominant influence on cutting forces, which directly govern the amount of material being removed. Variations in ***d*** also alter chip thickness and the tool-workpiece contact area, further affecting cutting forces and, consequently, part geometry. In contrast, feed rate and cutting speed primarily influence the material removal rate and thus have a comparatively smaller direct impact on radial *GD&T* parameters. Tool life (*TL*) is more strongly influenced by cutting speed (*V*), while surface roughness (***Ra***) is more strongly influenced by feed rate (***f***). These trends are more pronounced under dry cutting conditions than under *NFMQL*.

In summary, it is evident that the radial *GD&T* parameters, particularly cylindricity deviation, increase with depth of cut (***d***) and feed rate (***f***), but decrease with an increase in cutting speed (***V***). This trend is reflected in Eqs. (1)–(3) by the relatively high positive exponents for ***d*** and ***f*** (in that order) and the negative exponent for ***V***. These results confirm that depth of cut has the most significant effect on radial *GD&T* parameters, cutting speed primarily governs tool life, and feed rate is the dominant factor for surface roughness (***Ra***).

Cutting speed (***V***) has a substantial influence on both ***Ra*** and *TL*. The associated temperature rise at the cutting interface may increase the plasticity of the workpiece material, facilitating material removal and leading to lower ***Ra*** at higher ***V***. Increased speeds also typically reduce built-up edge formation on the cutting tool, which is a primary cause of dimensional errors and poor surface finish. Furthermore, higher cutting speeds promote smaller chip sizes and more continuous cutting, both of which enhance surface finish and geometric accuracy. The reduced contact time between the tool and workpiece at higher speeds may also minimize the time-dependent effects of frictional forces on workpiece distortion, thereby improving geometric accuracy.

However, higher speeds accelerate tool wear and increase the risk of cutting edge chipping as adhered material is more prone to detachment. Therefore, optimizing cutting speed is crucial to balance achievable surface quality with tool durability. The detrimental effect of high cutting speeds on tool wear can be mitigated by effective lubrication and cooling strategies, such as *NFMQL*. To gain a deeper understanding of tool performance, tool wear analysis for the *SPRT* is discussed further, taking into account the influence of cutting conditions.

Lower tool life and higher deviations in radial *GD&T* parameters at higher values of ***f*** and ***d*** can be attributed to increased cutting forces. These greater forces induce higher stress on the tool, leading to accelerated wear. They also generate more pronounced vibrations, which adversely affect surface finish and the precision of geometric features. In summary, higher values of feed rate and depth of cut result in elevated cutting forces and heat generation, which accelerate tool wear, degrade surface finish, and cause larger deviations in the geometric tolerances of the machined part.

Tool wear analysis

In the machining of *Inconel 718*, shear instability and localized deformation adversely affect tool wear, surface integrity, and overall machinability. An analysis of tool wear observed during turning with a custom-designed *SPRT* under *NFMQL* conditions is presented below.

The examination of worn tools under various machining conditions was conducted using digital microscopy and scanning electron microscopy (SEM), as shown in Fig. 8. The images depict the flank faces of tools after machining was terminated due to either catastrophic failure or upon reaching the flank wear limit of 0.2 mm.

Figs. 8, *a* and *b* show micrographs of the *SPRT* cutting edges from experimental runs ***R1*** and ***R5***, respectively. The cutting tools exhibit severe damage characterized by metal adhesion and pitting on the substrate. Chipping of the cutting edge, resulting from the fracture of adhered workpiece material, is clearly visible. This type of damage is more pronounced at higher cutting speeds. Furthermore, at higher ***V***, most tool failures were catastrophic, caused by edge chipping. The relatively minor metal adhesion observed at lower speeds can be attributed to reduced cutting temperatures, which inhibit temperature-dependent diffusion wear.

Figs. 9 and 10 present images along with the results of energy dispersive X-ray spectroscopy (*EDS*) analysis of the tool surfaces from runs ***R1*** and ***R5***, respectively. The elemental analysis (weight percent) from *EDS* confirms the adhesion of *Inconel 718* constituents onto the tool's rake surface. Significant pitting,

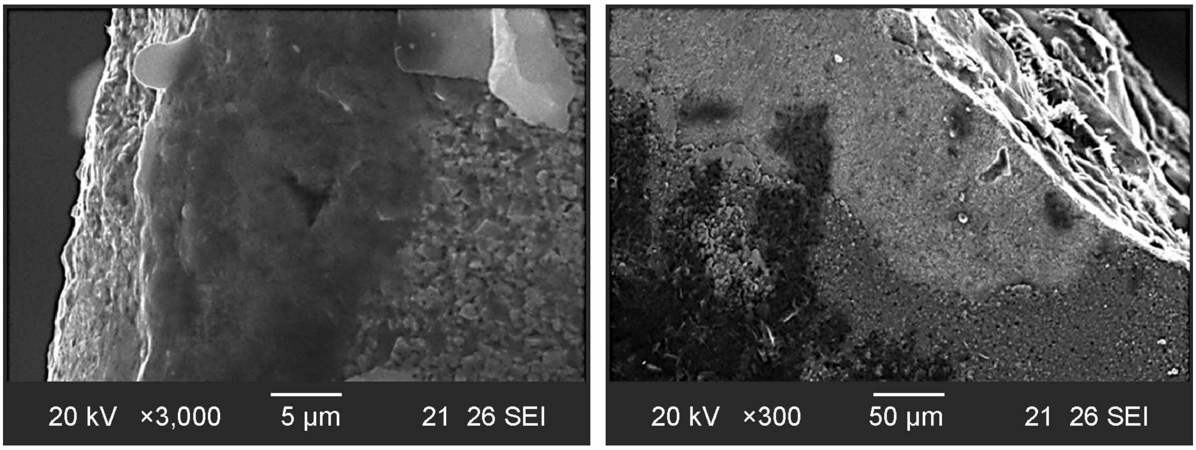

a *b*

Fig. 8. SEM images of tools at experimental runs *R*1 and *R*5

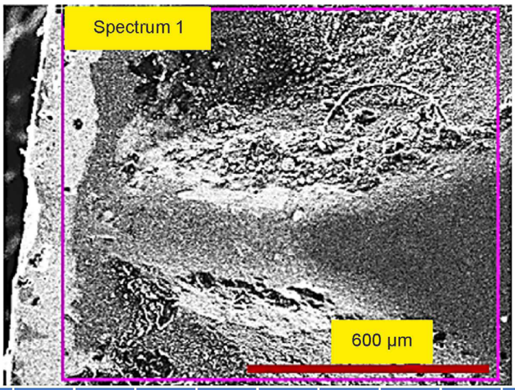

C	O	Al	Si	S	Ti	Cr	Fe	Ni	W
39.74	17.44	8.81	0.44	0.59	10.06	0.86	15.49	0.84	5.73

Fig. 9. Tool image with *EDS* analysis after experimental run *R*1

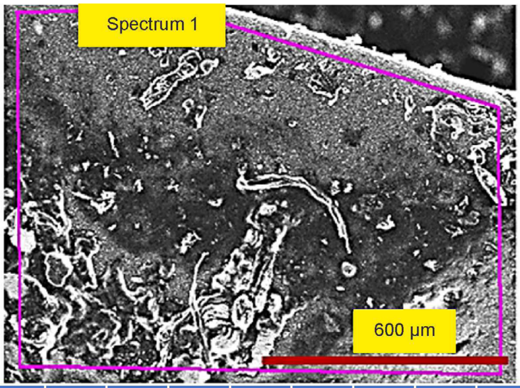

C	O	Al	Si	Cl	Ca	Ti	Cr	Fe	Co	Ni
60.56	17.05	8.48	0.34	0.18	0.24	10.28	0.52	0.63	0.48	1.25

Fig. 10. Tool image with *EDS* analysis after experimental run *R*5

plastic deformation, and destruction of the cutting edge with adhered metal are evident, particularly at higher cutting speeds. This demonstrates that cutting speed is a critical factor determining the severity of tool wear and the extent of metal adhesion during machining. These findings are consistent with those reported in [11–13].

Chip morphology produced during dry machining of *Inconel 718* with the *SPRT* is also discussed. The generated chips were continuously coiled, helical chips with a serrated (saw-tooth) edge. For nearly all cutting conditions considered in this study, tightly wound helical chips were produced. This characteristic was most prominent at higher cutting speeds (*V*). The present findings agree with those in [1, 7].

Chip curling is primarily influenced by the tool's thermal conductivity and the temperature gradient between the sliding and free surfaces of the chip. A larger temperature gradient leads to a smaller chip curl radius [7]. Fig. 11 shows the chip surfaces produced near the end of tool life in experimental runs ***R1*** and ***R5***. Chips generated by a severely worn tool exhibit significant damage, irregular plastic deformation, and abrasion marks on the free surface. This observation underscores the importance of timely tool replacement to maintain machining quality.

Multi-objective optimization

Experimental results indicate that for turning *Inconel 718* with an *SPRT*, depth of cut (***d***) is the most significant parameter for improving *GD&T* parameters, feed rate (***f***) is dominant for surface finish, and cutting speed (***V***) is most critical for tool life. Superior GD&T parameters and surface quality can be

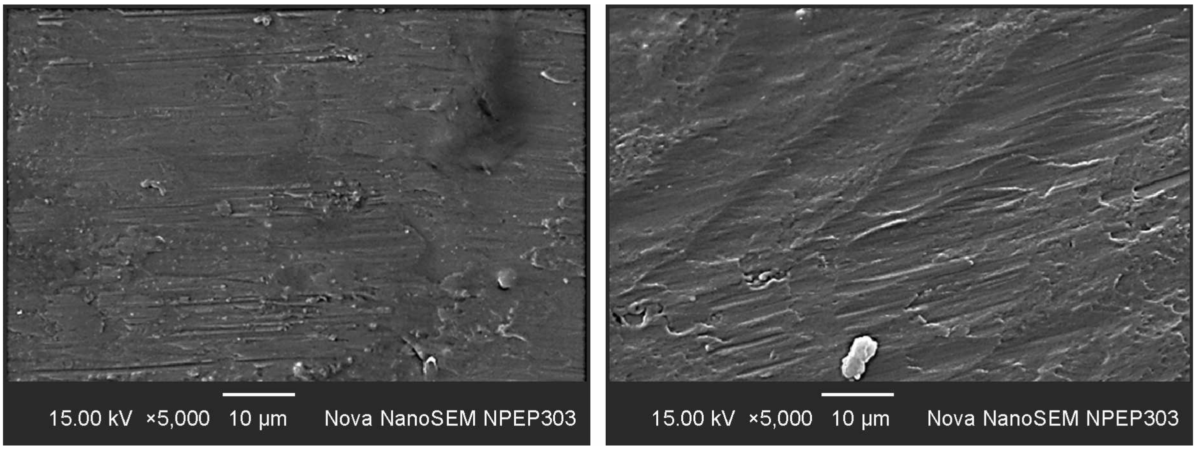

a *b*

Fig. 11. Chip images of the free surfaces after experimental runs *R*1 and *R*5

achieved by selecting smaller ***d*** and ***f*** combined with higher ***V***. Conversely, using lower cutting parameters promotes longer tool life. Thus, a conflict exists between achieving better part quality and extending tool life. Therefore, multi-parametric optimization is essential to simultaneously enhance all responses considered in this study.

A multi-objective genetic algorithm (*MOGA*) is effective for exploring the solution space. *MOGA* solutions are represented as a *Pareto* front. While genetic optimization yields multiple optimal trade-off solutions, identifying the single best compromise solution requires further analysis. Consequently, multi-criteria decision-making (*MCDM*) is essential for ranking the *Pareto*-optimal solutions. *MCDM* techniques enable the prioritization of solutions based on various criteria, facilitating the selection of the most suitable compromise. Thus, by integrating *MOGA* with *MCDM*, complex multi-objective decision-making can be streamlined to achieve an optimal compromise solution.

Here, the hybrid *Pareto*-based strategy *GA-TOPSIS*, used to analyze trade-offs and determine the optimal parameters is described [25]. The *GA-TOPSIS* method combines the *GA's* ability to explore a wide range of solutions with *TOPSIS's* ability to select the best compromise option. First, *GA* searches the parameter space and generates the *Pareto* front. Subsequently, *TOPSIS* ranks these options based on their proximity to an ideal solution.

The *GA*-based optimization was performed using the developed Eqs. (1) to (6) in *MATLAB*. The lower bounds for ***V***, ***f***, and ***d*** were set at (30, 0.1, 0.2) and the upper bounds at (65, 0.3, 0.8). The algorithm iteratively explores combinations within this range to find solutions that simultaneously optimize the conflicting objectives.

For the optimizer, the time, fitness, and stall time limits were not constrained. The stall generation limit was set to 100. Function and constraint tolerances were set to 1×10^{-4} and 1×10^{-3}, respectively, to achieve a good balance between solution accuracy and computation time. The *GA* was configured to terminate after approximately 200 generations. The remaining parameters of the multi-objective genetic optimizer were kept at their default settings. The population type was "*Double Vector*". A tournament selection function was used to increase the probability of selecting better solutions. Both forward migration and intermediate crossover were employed. This combination of operators promoted population diversity and adaptability, preventing premature convergence and encouraging thorough exploration of the search space.

Following optimization, the *Pareto*-optimal solutions generated by the *GA* are obtained. Table 5 displays the *Pareto* front, representing the set of non-dominated solutions. The *Pareto* front illustrates the trade-offs between objectives; any solution on the front cannot be improved in one objective without worsening another. This visualization aids in selecting the final optimal solution based on specific priorities [8, 25].

TOPSIS was then applied to identify the best compromise solution from the *Pareto* front in Table 5. A typical step in the *TOPSIS* method is to determine the positive ideal solution (*PIS*) and the negative ideal solution (*NIS*) [26]. Each alternative is evaluated based on its *Euclidean* distances to the *PIS* and the

Table 5

Genetic algorithm: *Pareto* solutions for *SPRT* under *NFMQL* conditions

Solution no.	*V* (m/min)	*f* (mm/rev)	*d* (mm)	Deviation in		*R/O* (mm)	*Ra* (μm)	*TL* (min)	*HRC*
				CIR (μm)	*CYL* (μm)				
1	30.00	0.10	0.20	4.03	10.51	0.23	1.39	8.44	36.26
2	60.91	0.11	0.20	3.80	8.28	0.16	1.07	3.69	38.03
3	63.56	0.30	0.80	9.03	59.31	0.69	1.73	1.50	39.20
4	62.98	0.20	0.46	6.44	27.40	0.39	1.44	2.11	38.77
5	59.58	0.30	0.77	8.91	57.94	0.69	1.76	1.65	39.01
6	61.90	0.23	0.70	8.04	46.21	0.58	1.58	1.79	38.91
7	60.69	0.17	0.61	7.09	35.27	0.47	1.43	2.14	38.63
8	64.84	0.30	0.80	9.03	59.02	0.68	1.72	1.47	39.25
9	64.84	0.30	0.80	9.03	59.02	0.68	1.72	1.47	39.25
10	63.35	0.29	0.70	8.46	50.81	0.61	1.69	1.59	39.14
11	30.05	0.10	0.40	5.68	23.83	0.43	1.54	6.53	36.47
12	59.49	0.13	0.22	4.12	9.92	0.18	1.15	3.46	38.10
13	61.56	0.30	0.75	8.79	55.83	0.66	1.73	1.60	39.09
14	60.44	0.18	0.35	5.46	18.82	0.30	1.35	2.56	38.50
15	58.59	0.28	0.65	8.14	47.06	0.59	1.70	1.82	38.88
16	59.57	0.29	0.49	7.10	33.80	0.46	1.64	1.95	38.86
17	63.35	0.29	0.71	8.48	51.15	0.62	1.69	1.59	39.14
18	30.00	0.10	0.20	4.03	10.51	0.23	1.39	8.44	36.26

NIS. The *PIS* maximizes benefit criteria and minimizes cost criteria, while the *NIS* does the opposite. The relative closeness of each alternative to the *PIS* is calculated. This closeness coefficient ranges from 0 to 1, where a value closer to 1 indicates a solution nearer to the ideal. The alternatives are ranked based on this coefficient, clearly identifying the best and worst compromise solutions from the *Pareto* set.

The detailed *TOPSIS* methodology employed in this work is described in [8, 11]. In the present study, the *GA*-generated solutions (Table 5) were first normalized. Each column of the normalized matrix was then multiplied by the corresponding weights of the output parameters to obtain the weighted normalized decision matrix. Subsequently, the positive ideal solution (*PIS*) and negative ideal solution (*NIS*) were determined. Next, the *Euclidean* distance of each alternative from the *PIS* and *NIS* was calculated. Finally, the relative closeness (proximity coefficient) for each alternative was computed.

To determine the objective weights for each response, the entropy weight method (*EWM*) was used. This method minimizes subjective bias by deriving weights directly from the data variability. A detailed procedure for calculating weights via *EWM* can be found in [8, 11]. The *GA-TOPSIS* approach identifies the solution that is farthest from the *NIS* and closest to the *PIS*.

Table 6 presents the normalized results and the weighted normalized matrix for the considered responses. Table 7 shows the *PIS*, *NIS*, separation measures (distances), proximity coefficients, and the resulting rank for each solution provided by *GA-TOPSIS*.

Based on the *GA-TOPSIS* results (Table 7), the top five ranked solutions – numbers 1, 18, 11, 2, and 12 – form a family of near-optimal solutions.

Table 8 presents the top five *GA-TOPSIS* solutions according to their rank. The results indicate that the optimal parameters for achieving superior turning performance of *Inconel 718* with an *SPRT* are ***V*** = 30 m/min, ***f*** = 0.1 mm/rev, and ***d*** = 0.2 mm. With these parameters, the following outcomes can be expected: a radial runout of 0.23 mm, circularity and cylindricity deviations of approximately 11 μm, a surface roughness (***Ra***) of 1.39 μm, a tool life of 8.44 min, and a workpiece hardness of 36.26 HRC.

Table 6

GA-TOPSIS: Normalized results and normalized weighted matrix for different responses for _SPRT_ under _NFMQL_ conditions

Solution no.	Normalized results ($\times 10^{-2}$) for						Normalized weighted matrix ($\times 10^{-2}$) for					
	CIR	*CYL*	*R/O*	R_a	*TL*	*HRC*	*CIR*	*CYL*	*R/O*	R_a	*TL*	*HRC*
1	13.11	5.97	10.70	21.15	53.03	22.23	2.18	1.00	1.78	3.51	8.92	3.68
2	12.37	4.71	7.28	16.18	23.19	23.32	2.05	0.79	1.21	2.68	3.90	3.86
3	29.41	33.71	31.47	26.24	9.44	24.03	4.89	5.64	5.24	4.35	1.59	3.98
4	20.96	15.58	17.68	21.78	13.23	23.77	3.48	2.61	2.95	3.61	2.23	3.94
5	29.00	32.93	31.50	26.71	10.33	23.92	4.82	5.51	5.25	4.43	1.74	3.96
6	26.17	26.26	26.31	23.96	11.24	23.86	4.35	4.40	4.38	3.97	1.89	3.95
7	23.09	20.05	21.62	21.64	13.44	23.68	3.84	3.36	3.60	3.59	2.26	3.93
8	29.38	33.54	31.17	26.05	9.22	24.06	4.88	5.61	5.19	4.32	1.55	3.99
9	29.38	33.54	31.17	26.05	9.22	24.06	4.88	5.61	5.19	4.32	1.55	3.99
10	27.54	28.88	28.04	25.68	9.98	24.00	4.58	4.83	4.67	4.26	1.68	3.98
11	18.50	13.55	19.78	23.43	41.02	22.36	3.07	2.27	3.30	3.89	6.90	3.71
12	13.41	5.64	8.39	17.43	21.70	23.36	2.23	0.94	1.40	2.89	3.65	3.87
13	28.60	31.73	30.35	26.24	10.05	23.96	4.75	5.31	5.06	4.35	1.69	3.97
14	17.79	10.70	13.50	20.50	16.07	23.60	2.96	1.79	2.25	3.40	2.70	3.91
15	26.49	26.75	27.08	25.79	11.42	23.84	4.40	4.48	4.51	4.28	1.92	3.95
16	23.12	19.21	21.02	24.92	12.24	23.83	3.84	3.22	3.50	4.13	2.06	3.95
17	27.61	29.07	28.18	25.70	9.96	24.00	4.59	4.87	4.70	4.26	1.67	3.98
18	13.11	5.97	10.70	21.15	53.03	22.23	2.18	1.00	1.78	3.51	8.92	3.68

Table 7

GA-TOPSIS: Optimal solutions for _SPRT_ under _NFMQL_ conditions

Solution no.	*V* (m/min)	*f* (mm/rev)	*d* (mm)	Separation measures ($\times 10^{-2}$)		Closeness coefficient (CC_i)	Rank
				S^+	S^+		
1	30.00	0.10	0.20	0.01	0.08	0.887	1
2	60.91	0.11	0.20	0.05	0.08	0.611	4
3	63.56	0.30	0.80	0.10	0.05	0.346	17
4	62.98	0.20	0.46	0.07	0.06	0.460	7
5	59.58	0.30	0.77	0.10	0.05	0.344	18
6	61.90	0.23	0.70	0.09	0.05	0.378	10
7	60.69	0.17	0.61	0.08	0.06	0.425	8
8	64.84	0.30	0.80	0.10	0.05	0.347	15
9	64.84	0.30	0.80	0.10	0.05	0.347	15
10	63.35	0.29	0.70	0.09	0.05	0.362	12
11	30.05	0.10	0.40	0.04	0.06	0.631	3
12	59.49	0.13	0.22	0.05	0.08	0.592	5
13	61.56	0.30	0.75	0.10	0.05	0.350	14
14	60.44	0.18	0.35	0.06	0.07	0.513	6
15	58.59	0.28	0.65	0.09	0.05	0.370	11
16	59.57	0.29	0.49	0.08	0.06	0.421	9
17	63.35	0.29	0.71	0.09	0.05	0.362	13
18	30.00	0.10	0.20	0.01	0.08	0.887	1

Table 8

GA-TOPSIS: Solutions ranked 1 to 5 for SPRT under NFMQL conditions

Rank	*V* (m/min)	*f* (mm/rev)	*d* (mm)	*CIR* (μm)	*CYL* (μm)	*R/O* (mm)	R_a (μm)	*TL* (min)	*HRC*
1	30.00	0.10	0.20	4.03	10.51	0.23	1.39	8.44	36.26
2	30.00	0.10	0.20	4.03	10.51	0.23	1.39	8.44	36.26
3	30.05	0.10	0.40	5.68	23.83	0.43	1.54	6.53	36.47
4	60.91	0.11	0.20	3.80	8.28	0.16	1.07	3.69	38.03
5	59.49	0.13	0.22	4.12	9.92	0.18	1.15	3.46	38.10

However, an alternative solution prioritizing part quality over tool life uses ***V*** = 61 m/min, ***f*** = 0.13 mm/rev, and ***d*** = 0.22 mm. This set of parameters yields lower deviations in circularity and cylindricity (limited to 8.28 μm), a reduced radial runout of 0.16 mm, a surface roughness of 1.07 μm, and a workpiece hardness of 38.03 HRC, albeit at the expense of a shorter tool life of 3.46 min.

To validate the optimization results, turning experiments were conducted using two distinct optimal cutting parameter sets, as detailed in Table 9. The reported values for surface roughness, tool life, workpiece hardness, and radial *GD&T* parameters are the averages from three consecutive experimental runs. The optimized predictions show good agreement with the experimental results, with an error margin of less than 10% for most of the investigated responses.

This study demonstrates that *Inconel 718* can be effectively machined with an *SPRT* using the following parameter ranges: a cutting speed of 30–60 m/min, a feed of 0.1 mm/rev, and a depth of cut of 0.2 mm. With these parameters, achievable outcomes include circularity and cylindricity deviations below 11 μm, radial runout below 0.23 mm, surface roughness (***Ra***) between 1.07 and 1.39 μm, tool life between 3.46 and 8.44 min, and workpiece hardness in the range of 36–38 HRC.

Table 9

Validation experiments for *SPRT* under *NFMQL* conditions

Performance measures	*GA-TOPSIS* prediction	Experimental results (repeated for three times)			Average experimental results	Average % error
		1st	2nd	3rd		
V = 30 m/min, ***f*** = 0.1 mm/rev, and ***d*** = 0.2 mm						
CIR (μm)	4.03	4.94	3.91	3.84	4.23	4.73
CYL (μm)	10.51	11.53	11.96	10.68	11.39	7.73
R/O (mm)	0.23	0.28	0.31	0.21	0.27	13.75
R_a (μm)	1.39	1.93	1.47	1.38	1.59	12.76
TL (min)	8.44	8.13	7.823	7.45	7.80	8.19
HRC	36.26	35.12	35.31	34.86	35.10	3.31
V = 61 m/min, ***f*** = 0.11 mm/rev, and ***d*** = 0.2 mm						
CIR (μm)	3.80	3.13	3.98	3.16	3.42	11.00
CYL (μm)	8.28	9.64	10.14	8.98	9.59	13.63
R/O (mm)	0.16	0.15	0.19	0.2	0.18	11.11
R_a (μm)	1.07	1.26	1.33	1.16	1.25	14.40
TL (min)	3.69	3.08	3.23	3.63	3.31	11.37
HRC	38.03	36.07	35.16	35.08	35.44	7.32

The findings of this study indicate that the use of *SPRT*s with hybrid Al_2O_3+*MWCNTs* nanofluid under *MQL* significantly enhances tool life compared to conventional round tools under dry cutting conditions [13]. This improvement can be attributed to enhanced heat transfer, facilitated by tool rotation and the superior thermal properties of the hybrid nanofluid.

However, only a marginal improvement in machining performance was observed for *SPRT*s under dry conditions versus those using the hybrid nanofluid [11]. Given these results, this study identifies potential for further enhancement of machining performance through the use of micro-textured self-propelled rotary tools in combination with various nanofluids under *MQL*, while also addressing machined surface integrity.

Conclusion

This work investigated and optimized surface roughness, subsurface hardness, tool life, and radial *GD&T* parameters (cylindricity, circularity, and radial runout) during the turning of *Inconel 718* with a self-propelled rotary tool (*SPRT*) using a hybrid *GA-TOPSIS* approach. The study leads to the following conclusions:

– A custom-designed *SPRT* was successfully used to turn *Inconel 718* and demonstrated a modest improvement in machining performance under *MQL* with nanofluid (*NFMQL*) conditions compared to dry turning. This is attributed to enhanced heat transfer and lubrication, facilitated by tool rotation and the effective cooling of the nanofluid.

– The depth of cut (***d***) was found to be the most significant parameter for improving radial *GD&T* parameters; feed rate (***f***) was the dominant factor for surface finish; and cutting speed (***V***) was the most critical for tool life.

– Mathematical models were developed from experimental data to analyze the influence of parameters on the responses. The models exhibit ***R***-squared values of approximately 0.95, indicating that they can provide valuable insights for process optimization during the turning of *Inconel 718*.

– Tool wear was predominantly characterized by a plastically deformed and damaged cutting edge with adhered workpiece material. Catastrophic failure via cutting edge chipping was the most common failure mode, particularly under severe cutting conditions.

– Chips produced at higher cutting parameters exhibited micro-deposits and parallel striations, whereas chips generated at lower parameters appeared polished.

– The *GA-TOPSIS* optimization revealed that superior turning of I*nconel 718* can be achieved with the *SPRT* using a cutting speed of 30–60 m/min, a feed of 0.1 mm/rev, and a depth of cut of 0.2 mm. With these parameters, achievable outcomes include circularity and cylindricity deviations below 11 µm, radial runout below 0.23 mm, surface roughness *(Ra)* between 1.07–1.39 µm, tool life between 3.46–8.44 min, and workpiece hardness of 36–38 HRC.

– This research provides valuable insights **r**elevant to the design of *SPRT*s and supports their broader adoption in machining of superalloys. The results can assist manufacturers in optimizing cutting parameters to enhance performance and efficiency when machining *Inconel 718*.

– The study also identifies a promising direction for future research: further improvement of machining performance under *MQL* using micro-textured *SPRT*s with different nanofluids, while paying close attention to machined surface integrity.

References

1. Rajurkar A., Chinchanikar S. Investigations on homothetic and hybrid micro-textured tools during turning Inconel-718. *Materials and Manufacturing Processes*, 2023, vol. 39 (4), pp. 529–545. DOI: 10.1080/10426914.2023.2236188.

2. Rajurkar A., Chinchanikar S. Investigation on the effect of laser parameters and hatch patterns on the dimensional accuracy of micro-dimple and micro-channel texture geometries. *International Journal on Interactive Design and Manufacturing*, 2024, vol. 18, pp. 7021–7038. DOI: 10.1007/s12008-023-01258-z.

3. Kulkarni P., Chinchanikar S. A review on machining of nickel-based superalloys using nanofluids under minimum quantity lubrication (NFMQL). *Journal of the Institution of Engineers (India): Series C*, 2023, vol. 104 (1), pp. 183–199. DOI: 10.1007/s40032-022-00905-w.

4. Shafiq A., Çolak A.B., Sindhu T.N. Significance of EMHD graphene oxide (GO) water ethylene glycol nanofluid flow in a Darcy–Forchheimer medium by machine learning algorithm. *The European Physical Journal Plus*, 2023, vol. 138 (3), p. 213. DOI: 10.1140/epjp/s13360-023-03798-5.

5. Chinchanikar S., Kore S.S., Hujare P. A review on nanofluids in minimum quantity lubrication machining. *Journal of Manufacturing Processes*, 2021, vol. 68 (A), pp. 56–70. DOI: 10.1016/j.jmapro.2021.05.028.

6. Faheem A., Husain T., Hasan F., Murtaza Q. Effect of nanoparticles in cutting fluid for structural machining of Inconel 718. *Advances in Materials and Processing Technologies*, 2022, vol. 8 (1), pp. 259–276. DOI: 10.1080/2374068X.2020.1802563.

7. Kulkarni P., Chinchanikar S. Machinability of Inconel 718 using unitary and hybrid nanofluids under minimum quantity lubrication. *Advances in Materials and Processing Technologies*, 2024, vol. 11 (1), pp. 421–449. DOI: 10.1080/2374068X.2024.2307103.

8. Kulkarni P., Chinchanikar S. Machining effects and multi-objective optimization in Inconel 718 turning with unitary and hybrid nanofluids under MQL. *Fracture and Structural Integrity*, 2024, vol. 18 (68), pp. 222–241. DOI: 10.3221/IGF-ESIS.68.15.

9. Makhesana M.A., Patel K.M. Performance assessment of vegetable oil-based nanofluid in Minimum Quantity Lubrication (MQL) during machining of Inconel 718. *Advances in Materials and Processing Technologies*, 2022, vol. 8 (3), pp. 3182–3198. DOI: 10.1080/2374068X.2021.1945305.

10. Ahmed W., Hegab H., Mohany A., Kishawy H. On machining hardened steel AISI 4140 with self-propelled rotary tools: experimental investigation and analysis. *The International Journal of Advanced Manufacturing Technology*, 2021, vol. 113 (11–12), pp. 3163–3176. DOI: 10.1007/s00170-021-06827-8.

11. Chinchanikar S., Motgi N. Machinability studies with radial GD&T parameters during turning Inconel 718 using a custom-designed self-propelled rotary tool: a GA-TOPSIS multi-objective optimisation approach. *Advances in Materials and Processing Technologies*, 2025, pp. 1–21. DOI: 10.1080/2374068X.2025.2497768.

12. Motgi N., Chinchanikar S. A review on self-propelled rotary tools: a comparative with fixed-tool machining, modeling, design, and developments. *Advances in Manufacturing Engineering: Select proceedings of ICFAMMT 2024*. Singapore, Springer, 2024, pp. 3–20. DOI: 10.1007/978-981-97-4324-7_1.

13. Chinchanikar S., Motgi N. Tool wear evaluation of self-propelled rotary tool and conventional round tool during turning Inconel 718. *Fracture and Structural Integrity*, 2024, vol. 18 (70), pp. 242–256. DOI: 10.3221/IGF-ESIS.70.14.

14. Li L., Kishawy H.A. A model for cutting forces generated during machining with self-propelled rotary tools. *International Journal of Machine Tools and Manufacture*, 2006, vol. 46 (12–13), pp. 1388–1394. DOI: 10.1016/j.ijmachtools.2005.10.003.

15. Emiroğlu U. Experimental study on turning with self-propelled rotary cutting tool. *Journal of Thermal Engineering*, 2017, vol. 3 (6), pp. 1553–1560.

16. Sasahara H., Kato A., Nakajima H., Yamamoto H., Muraki T., Tsutsumi M. High-speed rotary cutting of difficult-to-cut materials on multitasking lathe. *International Journal of Machine Tools and Manufacture*, 2008, vol. 48 (7–8), pp. 841–850. DOI: 10.1016/j.ijmachtools.2007.12.002.

17. Kossakowska J., Jemielniak K. Application of self-propelled rotary tools for turning of difficult-to-machine materials. *Procedia CIRP*, 2012, vol. 1, pp. 425–430. DOI: 10.1016/j.procir.2012.04.076.

18. Asokan P., Senthilkumaar J.S. Intelligent selection of machining parameters in turning of Inconel-718 using multi objective optimisation coupled with MADM. *International Journal of Machining and Machinability of Materials*, 2010, vol. 8 (1–2), pp. 209–225. DOI: 10.1504/IJMMM.2010.034497.

19. Mastan Rao P., Deva Raj C., Dhoria S.H., Vijaya M., Chowdary J.R.R. Multi-objective optimization of turning for nickel-based alloys using Taguchi-GRA and TOPSIS approaches. *Journal of the Institution of Engineers (India): Series D*, 2024, vol. 105 (3), pp. 1473–1484. DOI: 10.1007/s40033-023-00554-y.

20. Boumaza H., Belhadi S., Yallese M.A., Safi K., Haddad A. Optimization of surface roughness, tool wear and material removal rate in turning of Inconel 718 with ceramic composite tools using MCDM methods based on Taguchi methodology. *Sādhanā*, 2023, vol. 48 (1), p. 1. DOI: 10.1007/s12046-022-02060-5.

21. Zhou Q., Sivalingam V., Pandiyan K., Kumar G., Sun J. *Machinablity analysis and optimisation of process paramater in the turining of Inconel 718 alloy using multi criteria decision making method: A comparative study*. Springer Science and Business Media LLC, 2022, pp. 1–24. DOI: 10.21203/rs.3.rs-1542507/v1.

22. Ali M.A., Azmi A.I., Murad M.N., Zain M.Z., Khalil A.N., Shuaib N.A. Roles of new bio-based nanolubricants towards eco-friendly and improved machinability of Inconel 718 alloys. *Tribology International*, 2020, vol. 144, p. 106106. DOI: 10.1016/j.triboint.2019.106106.

23. Amrita M., Kamesh B. Optimization of graphene based minimum quantity lubrication of Inconel 718 turning with multiple machining performances. *Materials Today: Proceedings*, 2021, vol. 39 (4), pp. 1337–1344. DOI: 10.1016/j.matpr.2020.04.568.

24. Li B., Li C., Zhang Y., Wang Y., Yang M., Jia D., Zhang N., Wu Q. Effect of the physical properties of different vegetable oil-based nanofluids on MQLC grinding temperature of Ni-based alloy. *The International Journal of Advanced Manufacturing Technology*, 2017, vol. 89, pp. 3459–3474. DOI: 10.1007/s00170-016-9324-7.

25. Erkan Ö., Işık B., Çiçek A., Kara F. Prediction of damage factor in end milling of glass fibre reinforced plastic composites using artificial neural network. *Applied Composite Materials*, 2013, vol. 20, pp. 517–536. DOI: 10.1007/s10443-012-9286-3.

26. Sur G., Erkan Ö. Surface quality optimization of CFRP plates drilled with standard and step drill bits using TAGUCHI, TOPSIS and AHP method. *Engineering Computations*, 2021, vol. 38 (5), pp. 2163–2187. DOI: 10.1108/EC-04-2020-0202.

Conflicts of Interest

The authors declare no conflict of interest.